OPEN ACCESS
Journal of Innovative Optical Health Sciences
Vol. 14, No. 1 (2021) 2140011 (11 pages)

DOI: 10.1142/S1793545821400113

World Scientific
www.worldscientific.com

Automated retinal layer segmentation on optical coherence tomography image by combination of structure interpolation and lateral mean filtering

Yushu Ma*, Yingzhe Gao†, Zhaolin Li‡, Ang Li‡, Yi Wang‡, Jian Liu‡, Yao Yu‡, Wenbo Shi* and Zhenhe Ma‡,§

*School of Computer Science and Engineering
Northeastern University
Shenyang 110169, P. R. China

†Shenzhen Academy of Metrology & Quality Inspection
Shenzhen 518055, P. R. China

‡School of Control Engineering
Northeastern University at Qinhuangdao
Qinhuangdao 066004, P. R. China
§mazhenhe@163.com

Received 23 September 2020
Accepted 4 January 2021
Published 3 February 2021

Segmentation of layers in retinal images obtained by optical coherence tomography (OCT) has become an important clinical tool to diagnose ophthalmic diseases. However, due to the susceptibility to speckle noise and shadow of blood vessels etc., the layer segmentation technology based on a single image still fail to reach a satisfactory level. We propose a combination method of structure interpolation and lateral mean filtering (SI-LMF) to improve the signal-to-noise ratio based on one retinal image. Before performing one-dimensional lateral mean filtering to remove noise, structure interpolation was operated to eliminate thickness fluctuations. Then, we used boundary growth method to identify boundaries. Compared with existing segmentations, the method proposed in this paper requires less data and avoids the influence of microsaccade. The automatic segmentation method was verified on the spectral domain OCT volume images obtained from four normal objects, which successfully identified the boundaries of 10 physiological layers, consistent with the results based on the manual determination.

Keywords: Optical coherence tomography; retinal layers; automatic segmentation; mean filtering.

1. Introduction

Optical coherence tomography (OCT), which was first introduced in the early 1990s,[1] is an optical signal acquisition and processing modality which is noninvasive for imaging subsurface tissue structures. The extension of OCT into Fourier domain,

§Corresponding author.

for example, Fourier domain optical coherence tomography (FD-OCT),[2] has exploited its position in biomedical imaging applications, particularly in ophthalmology. OCT is now widely used in ophthalmic research and has been shown to be clinically useful in the diagnosis of a variety of retinal diseases.[3] For example, glaucoma can be determined by detecting the thickness of nerve fiber and ganglionic cell layers (NFL and GCL) using OCT.[6–8] Diabetic retinopathy is a continuing disorder of diabetes and endocrine system and blood system damage in the retina of a comprehensive reflection, is the main cause of vision loss.[9]

For better research and faster detection of these retinopathy-related diseases on specific types of cells within the retina, it is necessary to segment the different tissue layers existing in the retinal OCT images. Several methods have been proposed for the intra-retinal layer segmentation of OCT structural images. Koozekanani *et al.*[10] proposed an automatic algorithm that uses the edge detection kernel and the Markov model to segment the retinal boundary, from which the thickness of the retinal layer is obtained. Subsequently, other methods based on microstructural intensity and gradient or deformable spline algorithm to detect changes in reflectivity in the retinal substructure.[11] However, fully automated segmentation of intra-retinal layers in OCT is challenging because many factors affect the sharpness of layer boundaries and homogeneity of each layer.

Edge detection is a classic problem based on image intensity and its derivatives (gradient and Laplacian), segmentation based on edge detection is affected by image defects such as speckle noise and intensity discontinuity. As a result, many robust techniques have emerged to improve the accuracy of retinal segmentation. Gaussian filter[12] and multiple image averaging[13] are widely used to reduce speckle noise points and enhance the contrast between adjacent layer boundaries. However, Gaussian filter fuzzy boundaries reduce the contrast of two adjacent layers. Due to involuntary eye movements caused by microsaccades, image matching is a problem in the multi-image averaging. Fabritiuset *et al.*[14] presented a method to identify erroneous pixels by applying an automatic binarization algorithm following a top-hat filtering operation. However, their method is not always effective, especially when the retinal images are significantly inclined and the prior knowledge of the shape parameters of the morphological filter is not known. Fernández *et al.*[15] utilizing complex de-noising solutions apply nonlinear complex diffusion filtering with enhanced diffusion filtering techniques, and then locate the slope of the slope on the image. Ishikawa *et al.*[16] developed a software algorithm to perform automatic retinal layer segmentation in the macula of the commercially available Stratus TD-OCT, and reported that macular inner retinal layer thickness measurements could indeed be used to discriminate normal from glaucomatous eyes. Mishra *et al.*[17] proposed a two-step kernel-based optimization scheme that first located the approximate location of retinal layers using a gradient-based adaptive vector-valued kernel function and then optimized the segmentation using dynamic programming-based force balance equation to identify noisy layer boundaries. Ahlers *et al.*[18] applied the adaptive threshold and intensity peak detection to segment the layers of the retina. Xusheng Zhang *et al.*[11] performed a de-noising procedure with two steps of different Gaussian filtering, and proposed a two-step de-noising treatment in different directions to suppress random speckle noise while keeping the layer boundaries as complete as possible. However, the above segementation algorithms use an average number of graphs in denoising process or other methods to improve the signal-to-noise ratio that may fuzzy boundaries. Multiply images averaging require extra time and it is necessary for the patient to keep fixed during retinal information collection, which will make the patient feel uncomfortable, and the slight jitter caused by microsaccade may affect the image quality. Therefore, a novel denoising method based on a single OCT image and does not affect the sharpness of boundaries in pre-processing is great significance for retinal image segmentation.

In this paper, we propose a combination method SI-LMF to reduce the speckle noise and improve the signal-to-noise ratio to exploit an automatic retinal image segmentation method. First, all the retina layers are divided into upper and lower parts for processing based on layer ONL. The layers in the lower region gently floating was denoised by one dimensional lateral mean filtering (1D-LMF) and then identified by gradient value. The layers in the upper region big floating induced by the central fovea that directly using 1D-LMF will fuzzy boundaries. Therefore, structure interpolation was performed to eliminate layer floating before 1D-LMF. Next, we use boundary growth method to

identify the remaining layers. A segmentation result of an OCT retinal image from a health patient was exhibited to identify the accuracy of the method proposed in this paper. Compared with the traditional methods, our method takes less time for data collection and segmentation, and at the same time prevent the influence of microsaccade.

2. Experimental Setup

To verify the accuracy and practicability of the proposed method, a typical SDOCT system is employed in this paper (schematic is shown in Fig. 1), similar to the described in our previous study.[19] Briefly, the system provides both structural and phase images of retinal layers. The light source is a superluminescent diode (D-840-HP-I, Superlum) centered at 840 nm with a full width at half maximum bandwidth of $\sim$45 nm, providing an axial resolution of $\sim$7 μm in air. The light goes through a circulator and is split into two beams by a 2×2 fiber coupler. In the sample arm, the beam routed through a collimating lens, X-Y galvanometers and an objective lens with 50 mm which provides $\sim$16 μm lateral resolution. To provide sufficient lateral length, space of two adjacent A-scans was set as $\sim$6 μm and each B-scan was formed by 500 A-scans covering 3 mm. The interference spectrum of light backscattered from reference and sample arms was captured by a home-built spectrometer which utilizes a high speed line scan camera. The line scan rate of the camera can run as high as 70k lines per second in this study.

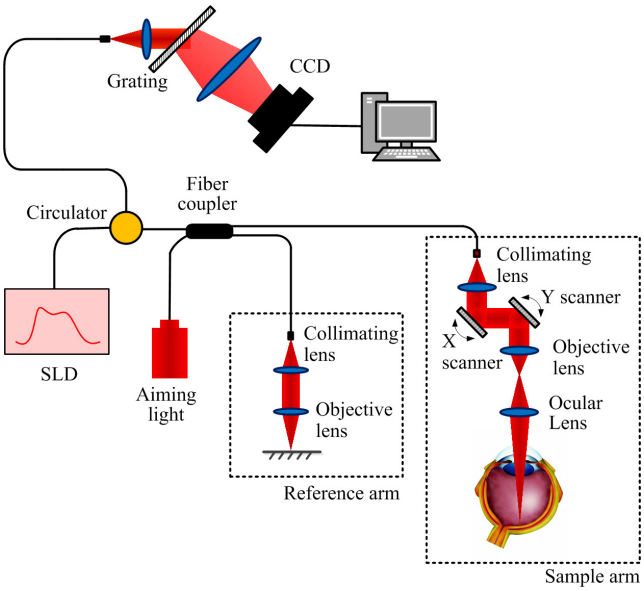

Fig. 1. Schematic of the OCT imaging system.

3. Method

3.1. *Method overview*

Figure 2 shows a cross-sectional OCT structure image of the retina centered at the macula, annotated with the targeted 10-layer boundaries. The abbreviations of layers from top to bottom are: ILM — inner limiting membrane, NFL — nerve fiber layer, GCL — ganglion cell layer, IPL — inner plexiform layer, INL — inner nuclear layer, OPL — outer plexiform layer, ONL — outer nuclear layer, IS — photoreceptor inner segment, OS — photoreceptor outer segment, OSJ — outer segment junction and RPE — retinal pigment epithelium.

The schematic diagram of segmentation steps is shown in Fig. 3. Briefly, it includes five steps: (1) Image rotation based on the RPE centerline; (2) ILM identification; (3) ONL determination and separate layers to two regions (above and beneath ONL); (4) layers segmentation beneath ONL layer depend on 1D-LMF; (5) Layers segmentation above ONL layer depending on SI-LMF.

3.2. *Image rotation based on the RPE layer centerline*

Since the incident beam of the OCT imaging system is not always perpendicular to the fundus, the structure image of the retinal layers may have a random tilt angle, so image rotation is a prerequisite before subsequent segmentation.

In healthy human fundus, the RPE layer fluctuates slowly, and the backscattered light of RPE layer is one of the largest in retinal OCT image. Therefore, we rotate the image perpendicular substantially to the Z-direction based on a pilot estimate of the RPE centerline. The RPE centerline is identified by tentatively assigning the brightest pixel in each column. However, the automatic selection is not perfect due to the presence of noise points. Majority of erroneous pixels are usually associated with the layer NFL and layer OS which also exhibits high reflective in the OCT image.[20–22] Since the layer NFL and layer OS are not adjacent to layer RPE, it is possible to reduce the deviation by removing discontinuities greater than 14 pixels in the RPE estimate.[22] The size of the filter is

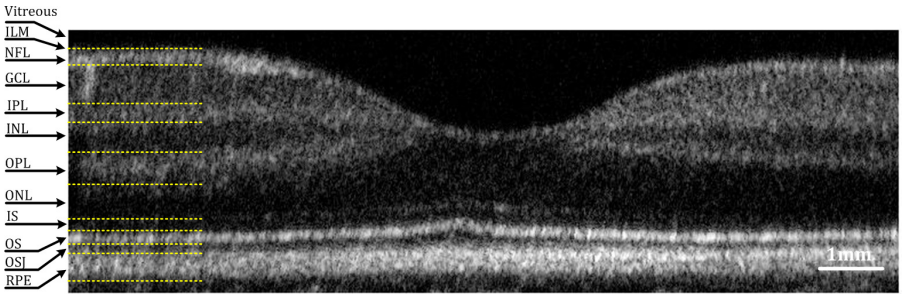

Fig. 2. Target retinal layers of a B-scan SDOCT image.

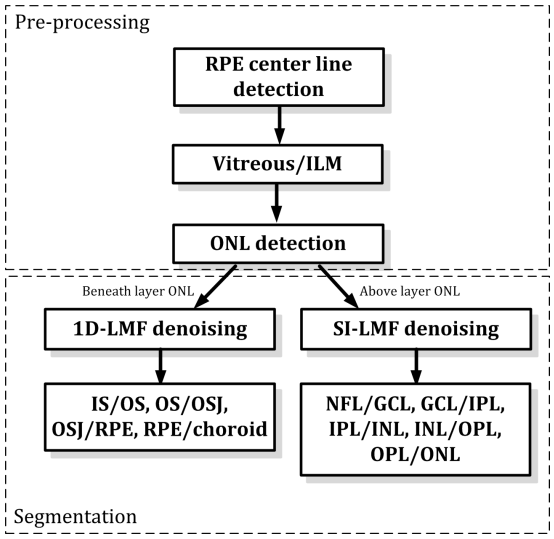

Fig. 3. Schematic of layers segmentation.

connected to the width of RPE layer and thus they must be adjusted if scanning protocol is changed. The remaining valid points were smoothed by a moving average median filter with a window size of 40, as shown in Fig 4(a).

In order to improve the accuracy of the angle in adjusting image, the RPE centerline was fitted to a first-order polynomial. Based on the averaging slope of the polynomials, the retinal OCT image was rotated perpendicular to the Z-direction to facilitate subsequent segmentation. Regions of the horizontal image outside the original field were cut off (outside of red rectangle in Fig 4(b)]. The remaining part was cropped from the rotated OCT image and shown in Fig. 4(c).

3.3. *Vitreous/ILM boundary segmentation*

The vitreous/ILM is the boundary between the vitreous body and the retina. Since there is no high scattering of the interferential blood vessels or absorbing tissues above layer ILM, the ILM identification can be performed easier than other layers. The vitreous/ILM boundary was segmented by searching for the greatest contrast rise in the region above the RPE centerline. The error points in the OCT image were eliminated by statistical regression

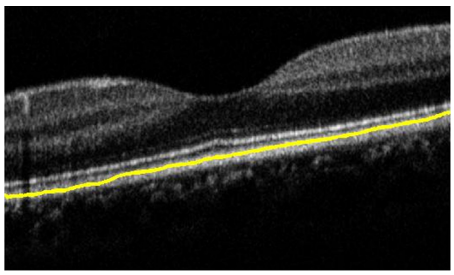

(a)

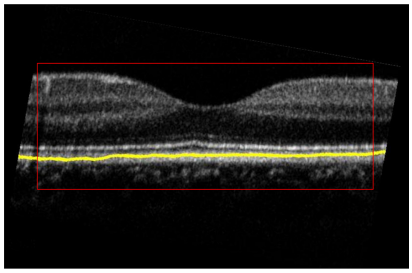

(b)

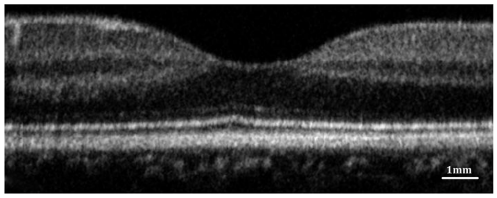

(c)

Fig. 4. Image rotation based on RPE centerline. (a) Retinal OCT image with RPE centerline; (b) Image after rotation. (c) Cropped OCT image.

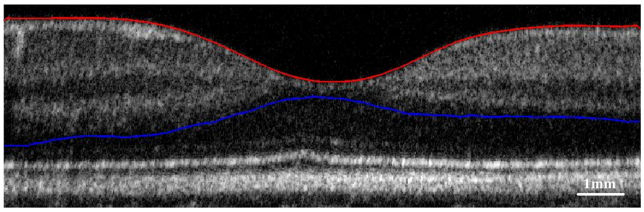

Fig. 5. Segmentation results of vitreous/ILM boundary and layer ONL

method, and the resulted line is smoothed by an eight-order fitting polynomial (red line in Fig. 5).

3.4. *ONL segmentation and two parts (above and beneath ONL) division*

The ONL is the thickest layer with minimal backscattering intensity in the retina. Since the search area is limited by the prior segmented layers, layer ONL is easy to identify. In each A-line, the ONL layer is defined by searching for the minimum intensity point between the vitreous/ILM boundary and RPE centerline. All the selected points were combined into a curve and smoothed with the adjustment procedure described above to reduce error points. The segmentation result of ONL layer is shown in Fig. 5 (blue line).

After determining the layer ONL, the retina was divided into two different parts. The layers between layer ONL and end of layer RPE are almost parallel to each other. The lower region was directly denoised by 1D-LMF to reduce speckle noise and improve the signal-to-noise ratio, then the layers beneath layer ONL were segmented according to the gradient value. For the structure above layer ONL, layers merge together and become increasingly difficult to distinguish in the region close to fovea. To eliminate the influence of layer floating caused by the central fovea, structure interpolation was operated before the 1D-LMF procedure. We call this combination method, structure interpolation and lateral mean filtering (SI-LMF). Layers above layer ONL was identified by boundary growth method.

3.5. *Layers segmentation beneath layer ONL*

3.5.1. *1D-LMF denoising*

The boundaries between layer ONL and RPE were densely located, and speckle noise caused by self-coherence deteriorated the structure image. To improve the signal-to-noise ratio of OCT images, image de-noising is an essential procedure to improve accuracy of segmentation.

We adopted two denoising methods, horizontal 1D-LMF and two-dimension Gaussian filter. The window size of 1D-LMF is 1*11 and Gaussian filter is 3*3, sigma is 1. Since the contrast of the layers beneath layer ONL is high, both Gaussian filter and 1D-LMF can be used to reduce noise pixels. Based on the structure feature, the layer boundaries between ONL and RPE are closely being parallel, and the fluctuation of layers can be ignored in local areas. Figure 6 exhibits denoising results of two methods. We can see that Fig 6(c) (denoised by 1D-LMF) have fewer speckle noise and clearer boundaries (layers beneath ONL). To observe the ability of noise reduction in details, A-lines in same lateral position [yellow line in Figs. 6(a)–6(c)] were selected

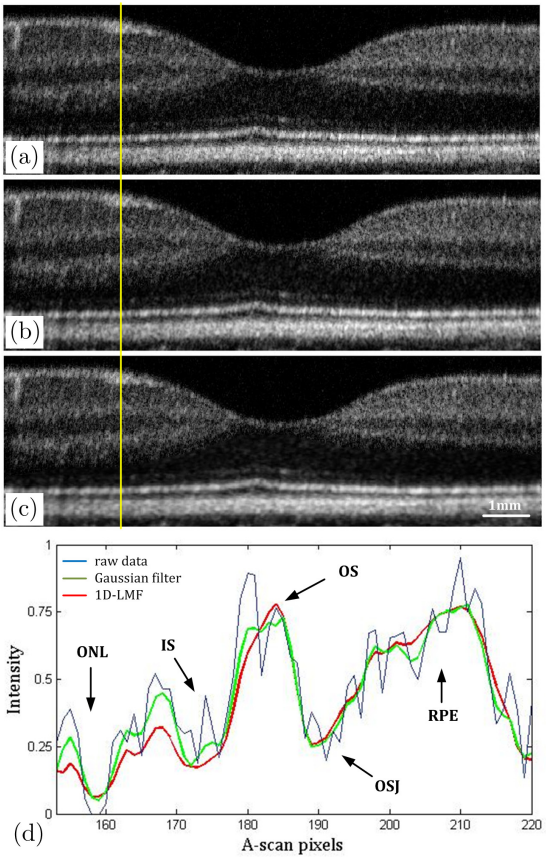

Fig. 6. De-noising results and intensity information of selected an A-line from one B-frame. (a) raw B-frame, (b) denoised by Gaussian filter, (c) denoised by the 1D-LMF, (d) is the intensity profiles of yellow line in the image (a)(b)(c) were shown by blue, green and red lines.

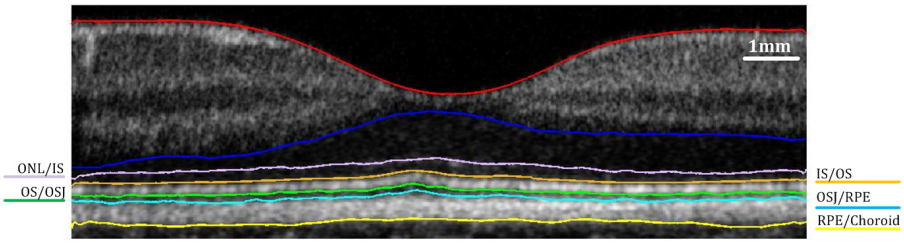

Fig. 7. Segmentation results of boundaries beneath layer ONL. From top to bottom, lines are ONL/IS, IS/OS, OS/OSJ, OSJ/RPE and RPE/Choroid.

and intensity distributions were compared in Fig 6(d), the red curve is much smoother than green curve. All the results show that the performance of 1D-LMF in denoising speckle noise is slightly better than Gaussian filter. After noise reduction of the raw image, identifying layers beneath layer ONL becomes easier.

3.5.2. *Segmentation of layers IS, OS, OSJ and RPE*

After the de-noising procedure in previous section, the layers beneath layer ONL were easily identified. First, begin and end of layer OS were confirmed by searching for the maximum contrast rise and drop, respectively, with the search area being limited between layer ONL and RPE centerline. Once the layer OS was confirmed, the ONL/IS boundary was selected by searching for the maximum intensity pixels between layer ONL and begin of layer OS. Then, OSJ/RPE boundary is selected by searching for the largest contrast rise between the end of OS and RPE centerline. Since the intensity of layer RPE is high and the choroid region is small, the end of RPE was obtained by searching for the maximum contrast drop beneath the RPE centerline. Figure 7 shows the segmentation results of layers ONL, IS, OS, OSJ and RPE.

3.6. *Layers segmentation above layer ONL*

3.6.1. *SI-LMF denoising*

Vessels between layer ILM and ONL are relatively abundant, especially in layer GCL. Both vascular structure and the shadow of blood flow will cause elongated and disjoint spots in OCT images, which interfere with the segmentation of boundaries. Since the vessels are mostly isolated in the cross-sectional image, related interference could be grossly eliminated by 1D-LMF. However, the thickness of layers above layer ONL varies significantly, especially near the foveal region. Therefore, simple horizontal average inevitably leads to fuzzy structure and difficulty in distinguishing boundaries. Thus, the structure interpolation which eliminate the influence of layer thickness floating caused by the central fovea is indispensable before 1D-LMF, i.e., the SI-LMF method proposed in this paper.

First of all, structure between vitreous/ILM boundary and layer ONL of each A-line was resized to same thickness [Fig. 8(b)]. The vitreous/ILM boundary and layer ONL which have been identified in previous step 3.3. After structure resizing, we assume that all the boundaries above layer ONL are parallel. Then, 1D-LMF was performed similar to Sec. 3.5.1, and the result is shown in Fig. 8(c). Then, the averaged structure was resized back to the initial size and replaced the original location in raw image [Fig. 8(d)]. To verify the de-noising ability of SI-LMF, A-lines of same lateral position were selected from raw image [Fig. 8(a)], SI-LMF result [Fig. 8(d)] and Gaussian filter result [Fig. 8(e)]. We can see that there is a small blood vessel in the GCL layer [red arrow in Fig. 8(a)]. Correspondingly, there is a peak in Fig. 8(f) (blue circle), which is prone to be recognized as a wrong layer in boundary segmentation. Since blood vessels are thin, the proposed algorithm smoothed the structure with intensity average. The peak was eliminated after 1D-LMF [red line in Fig. 8(f)], while the peak is retained after Gaussian filtering [green line in Fig. 8(f)].

After the de-noising step, boundaries were automatically segmented by the peak point of the gradient value in each A-line. The advantage of identifying gradient instead of intensity information is that the result will not be severely affected by local absolute intensity values as long as the contrast between layers remains. Figure 9 shows the rough segmentation results based on different

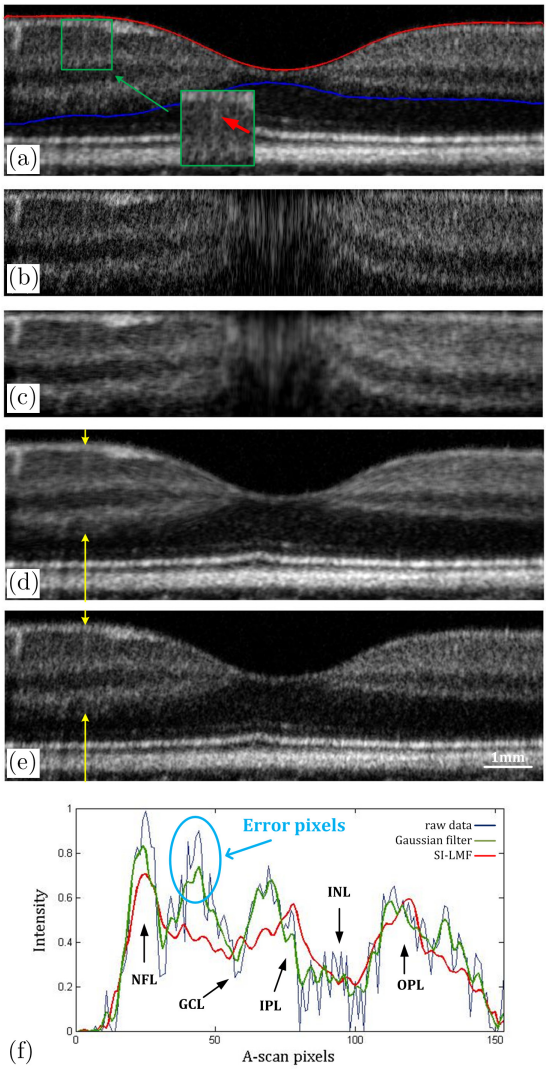

Fig. 8. Interpolation step. (a) Raw OCT image with vitreous/ILM boundary and layer ONL. Green square, interested region. (b) Resize the interested region to same width. (c) Reducing error points with 1D-LMF. (d) Resize de-noising result back to original size and replace the same position in raw image. (e) Reducing error points with Gaussian filter. (f) Selected an A-line from raw image (blue line), image with Gaussian filter (green line) and with SI-LMF (red line). Blue circle, error pixels caused by retinal vessels which are eliminated by SI-LMF.

images: (a) the image using Gaussian filter, (b) the image using SI-LMF. The comparison verified the effectiveness of SI-LMF.

3.6.2. *Boundary growth method*

In Fig. 9(b), five boundaries are roughly segmented between vitreous/ILM boundary and layer ONL. However, isolated points still present which can interfere with automatic segmentation. To

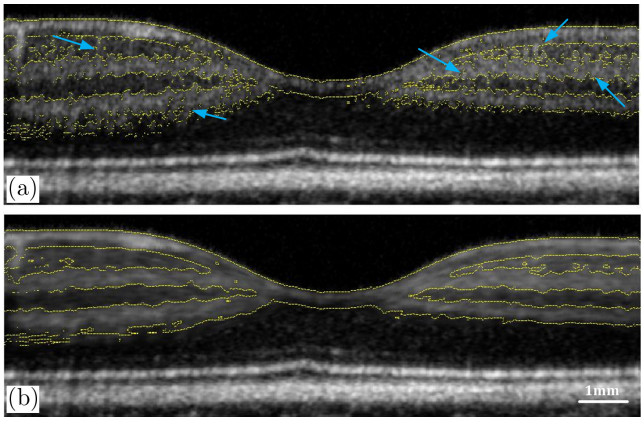

Fig. 9. Performance of SI-LMF in boundaries above layer ONL. (a) Searching for the peak of the gradient value of a raw OCT image and (b) a de-noising image with SI-LMF. Blue arrow, error points caused by scattered vessels.

eliminate those error pixels, the boundary growth method was used. First, two groups of precise initial points were selected based on the gradient value around the left and right border of the retina image. Each group contains six points, corresponding to correct layer boundaries on the selected A-line. Initial points group need to satisfy two criterions: (1) there are only six edge points at that lateral position (A-line); (2) the interval between each adjacent two points is sufficient. Once we obtained the two group of initial points (shown in Fig. 10), search the point from the basis A-line to the ipsilateral edge and the center of the image.

Once two groups of initial points were confirmed, boundary started to grow towards both sides. This was realized by searching the closest edge pixel on the adjacent two A-lines in Fig. 11(a). Due to the error pixels interference the searching result, a threshold was set to limit the search area. If there is no edge point in the range, the boundary position on the next A-line was set the same as the previous position. Figure 11(b) shows the five boundaries corrected with boundary growth method. All segmentation boundaries were slightly smoothed with

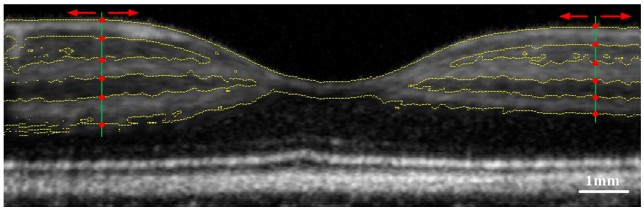

Fig. 10. Two group of initial points.

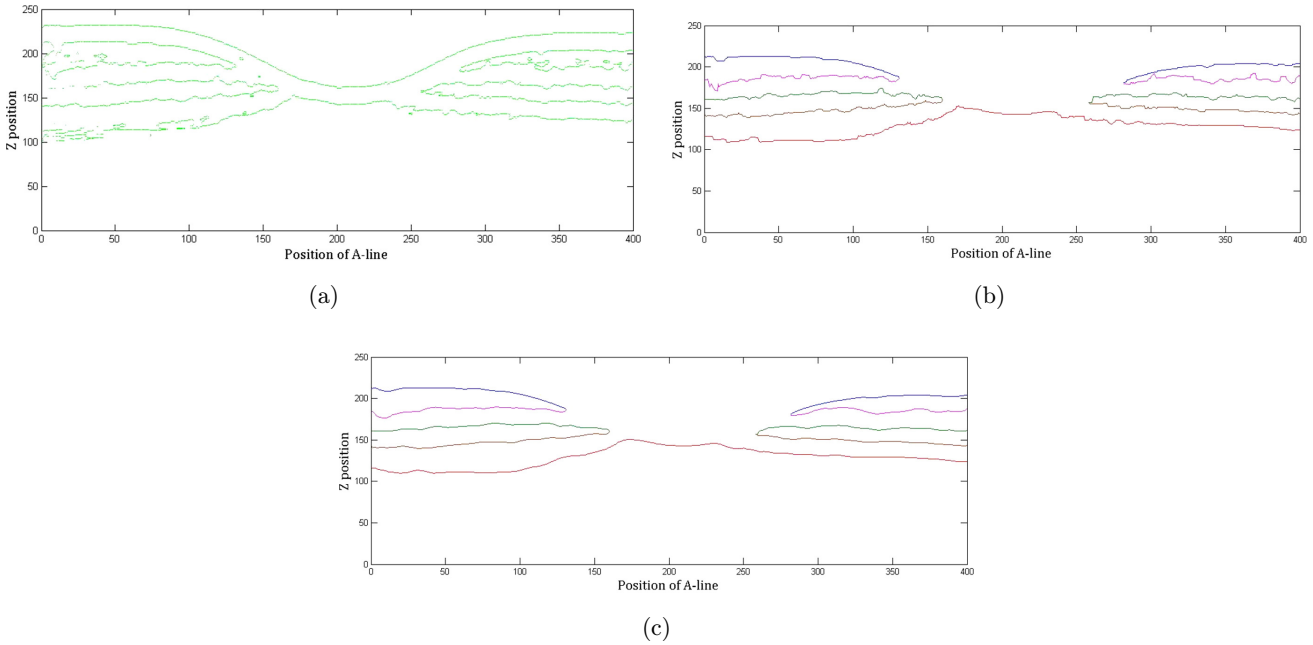

Fig. 11. Illustration of layer growth method. (a) Peak points of the gradient value of a typical OCT image. (b) Correct automation segmentation pixels with layer growth algorithm. (c) Smoothing with moving average median filter.

a moving average median filter with a window size of 20.

4. Results

To verify the accuracy of segmentation algorithm on OCT image, we applied the method to the datasets of four volunteers (Table 1) in our lab. 10 retinal layers (NFL, GCL, IPL, INL, OPL, ONL, IS, OS, OSJ, RPE) were segmented automatically in 20 B-scans using a MATLAB (The MathWorks, Inc.) software implementation of our method. The average calculation time for each image running on a personal computer (64bit Windows, Intel Core i7 CPU at 3.6 GHz, and 8GM RAM) is 3.6 s. The segmented results of 10 layers with the algorithm described in Sec. 3 are illustrated in Fig. 12 for one of the typical B-frames.

Table 1. Baseline information of four volunteers.

Volunteer	Age	Gender
1	20	Female
2	22	Male
3	26	Male
4	28	Female

50pcs B-scan images were obtained for each volunteer. The poor-quality frames with low contrasts or obvious motion artifacts were discarded before segmentation. Then, nine images were randomly selected for analysis. Same 10 layers were manually traced by an independent physician for the subset of

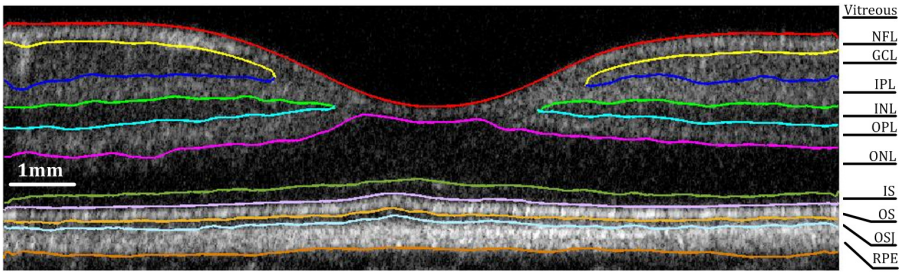

Fig. 12. Segmentation results of all 10 layers. From top to bottom, layer NFL, GCL, IPL, INL, OPL, ONL, IS, OS, OSJ, RPE.

Table 2. Differences between manual and automatic segmentation. 2.3 μm/pixel.

Layer	Mean difference (pixels)	SD (pixels)
NFL	0.53	1.2
GCL	−0.44	0.54
IPL	0.65	1.625
INL	0.85	0.66
OPL	−1.57	1.02
ONL-IS	1.79	1.6
OS-OSJ	−0.46	0.48
RPE	−1.14	0.6

36 B-scans. Table 2 lists the absolute mean and standard deviation (SD) of the differences between manual and automatic estimates of the segmentation data. Each pixel is 2.3 μm. It is noted that the SD of IPL and ONL-IS are greater among all the layers. This is because contrast is poor and boundary is fuzzy at the beginning of layer IPL and two sides of layer ONL. In structural image, the boundaries of GCL/IPL and ONL/IS are vague and difficult for segmentation. In some segmentation algorithms, GCL/IPL was integrated as one layer[11,20] and ONL/IS was integrated as one layer.[20,23]

5. Discussion

Compared with traditional pre-denoising method such as Gaussian filter and averaging multiple images, since the layers under the layer ONL are parallel to each other, the segmentation results of the bottom region are similar. In the top part of retina, the SI-LMF de-noising method exhibits a better recognition effect, especially in areas with abundant blood vessels. The method proposed in this paper performs well in eliminating speckles in a single plot. Compared with other existing methods, the proposed method does not rely on a large amount of data or multiple images, thereby saving lots of time for searching error pixels and improving the sharpness of boundaries in OCT images.

Accurate detection of anatomical and pathological structures in SDOCT images is critical for the diagnosis of ocular diseases. Automatic fundus segmentation is challenging due to the presence of speckle noise, vessel shadows and layer structure fluctuations. Many methods have been proposed to identify the retinal layers, which are mainly divided into two classes: traditional image processing and deep learning. Generally, segmentation algorithms based on image processing require multiple steps, including pretreatment and step-by-step identification of layers which are time consuming. In recent years, some new segmentation algorithms based on deep learning were developed to identify retinal layers.[23,24] Those algorithms can save a lot of manpower and segment OCT retinal images in a short time after training. However, all types of deep learning algorithms require large amounts of data for training, which is hard to obtain. The proposed method uses only one OCT image to segment retinal layers and is easy to be implemented. The combination of traditional segmentation methods and deep learning is a trend, which can improve accuracy.[23] In the future, we may also consider combining the methods in this paper with machine learning.

SI-LMF performances good in minimizing the influence of the scattered blood vessels and their corresponding shadows in de-noising step. However, it is difficult to eliminate some error pixels caused by large blood vessels, especially those close to the layer boundaries. For the boundary growth method, current boundary pixel determination depends on the location of previous pixel. Therefore, initial boundary points selection is critical to segmentation accuracy. Simultaneously, error pixels from irregular boundary points will lead to poor results or failure of the segmentation algorithm.

The determination of thickness and the junction boundary of retinal layers obtained by OCT system has been widely used to diagnose ophthalmic diseases such as glaucoma and retinitis pigmentosa.[25,26] The SI-LMF method overlaying pixels in a small range might slightly weaken the abnormal morphological structure caused by the diseases. However, the lesion of boundaries between two layers mostly occur in the later stage. It is well known that the measurement of thickness at early stage of retinal diseases is meaningful and it could be treated effectively.

In summary, the SI-LMF-based automatic segmentation method can reduce the number of images that need to be collected, save time and improve the accuracy. It can be used as a convenient and fast diagnostic tool to identify 10-layer by a single OCT retinal images.

Conflict of Interest

The authors have no conflicts of interest relevant to this article.

Acknowledgments

This work was supported in part by National Natural Science Foundation of China (61771119 and 61901100), Hebei Provincial Natural Science Foundation of China (H2018501087 and H2019501010). Fundamental Research Funds for the Central Universities (N182304008).

References

1. D. Huang *et al.*, "Optical coherence tomography," *Science* **254**(5035), 1178–1181 (1991).
2. S. H. Yun *et al.*, "High-speed spectral-domain optical coherence tomography at 1.3 μm wavelength," *Opt. Express* **11**(26), 3598–3604 (2003).
3. R. N. Weinreb, L. Zangwill, "Reproducibility of nerve fiber layer thickness measurements using 3D Fourier-domain OCT," *Ophthalmology* **104**(10), 1530–1531 (1997).
4. S. Alam, R. J. Zawadzki, S. Choi *et al.*, "Clinical application of rapid serial Fourier-domain optical coherence tomography for macular imaging," *Ophthalmology* **113**(8), 1425–1431 (2006).
5. W. Maciej *et al.*, "Three-dimensional retinal imaging with high-speed ultrahigh-resolution optical coherence tomography," *Ophthalmology* **112**(10), 1734–1746 (2005).
6. E. Garcia-Martin, M. Satue, I. Fuertes *et al.*, "Ability and reproducibility of Fourier-domain optical coherence tomography to detect retinal nerve fiber layer atrophy in Parkinson's disease," *Ophthalmology* **119**(10), 2161–2167 (2012).
7. Divya, Aggarwal, Ou, "Patterns of ganglion cell complex and nerve fiber layer loss in nonarteritic ischemic optic neuropathy by Fourier-domain optical coherence tomography," *Investig. Opthalmol. Vis. Sci.* **53**(8), 4539 (2012).
8. O. Tan, V. Chopra, T. H. Lu *et al.*, "Detection of macular ganglion cell loss in glaucoma by Fourier-domain optical coherence tomography," *Ophthalmology* **116**(12), 2305–2314.e2 (2009).
9. T. Qaum, Q. Xu, A. M. Joussen *et al.*, "VEGF-initiated blood-retinal barrier breakdown in early diabetes," *Investig. Ophthalmol. Vis. Sci.* **42**(10), 2408 (2001).
10. D. Koozekanani, K. Boyer, C. Roberts, "Retinal thickness measurements from optical coherence tomography using a Markov boundary model," *IEEE Trans. Med. Imaging* **20**(9), 900 (2001).
11. X. Zhang, S. Yousefi, L. An *et al.*, "Automated segmentation of intramacular layers in Fourier domain optical coherence tomography structural images from normal subjects," *J. Biomed. Optics* **17**(4), 046011 (2012).
12. Y. Wang, T. Li, "Image de-noising using wavelet transform and various filters," *Int. J. Re. Computer Sci.* **2**(2), 1–7 (2012).
13. A. Sakamoto, M. Hangai, N. Yoshimura, "Spectral-domain optical coherence tomography with multiple B-scan averaging for enhanced imaging of retinal diseases," *Ophthalmology* **115**(6), 1071–1078.e7 (2008).
14. T. Fabritius, S. Makita, M. Miura *et al.*, "Automated segmentation of the macula by optical coherence tomography," *Opt. Express* **17**(18), 15659–15669.
15. F. D. Cabrera, H. M. Salinas, C. A. Puliafito, "Automated detection of retinal layer structures on optical coherence tomography images," *Opt. Express* **13**(25), 10200 (2005).
16. H. Ishikawa, D. M. Stein, G. Wollstein *et al.*, "Macular segmentation with optical coherence tomography," *Investig. Ophthalmol. Vis. Sci.* **46**(6), 2012–2017 (2005).
17. A. Mishra, A. Wong, K. Bizheva *et al.*, "Intra-retinal layer segmentation in optical coherence tomography images," *Optics Express* **17**(26), 23719–23728 (2009).
18. C. Ahlers, C. Simader, W. Geitzenauer *et al.*, "Automatic segmentation in three-dimensional analysis of fibrovascular pigment epithelial detachment using high-definition optical coherence tomography," *Br. J. Ophthalmol.* **92**(2), 197 (2008).
19. Y. Zhao, Y. Ma, J. Liu *et al.*, "Phase unwrapping for Doppler Spectral Domain OCT flow measurement," *J. Biophotonics* **13**(1) (2019).
20. S. J. Chiu, X. T. Li, P. Nicholas *et al.*, "Automatic segmentation of seven retinal layers in SDOCT images congruent with expert manual segmentation," *Opt. Express* **18**(18), 19413–19428.
21. S. Lu, Y. L. Cheung, J. Liu *et al.*, "Automated layer segmentation of optical coherence tomography images," *IEEE Trans. Biomed. Eng.* **57**(10), P.2605–P.2608 (2010).
22. J. Tian, B. Varga, G. M. Somfai *et al.*, "Real-time automatic segmentation of optical coherence tomography volume data of the macular region," *Plos One* **10**(8), e0133908 (2015).
23. Z. Mishra, A. Ganegoda, J. Selicha *et al.*, "Automated retinal layer segmentation using graph-based algorithm incorporating deep-learning-derived information," *Sci. Rep.* **10**, 9541 (2020).

24. K. Gopinath, S. B. Rangrej, J. Sivaswamy, "A deep learning framework for segmentation of retinal layers from OCT images," *2017 4th IAPR Asian Conference on Pattern Recognition (ACPR)*, Nanjing, 2017, pp. 888–893.
25. C. K. Leung *et al.*, "Evaluation of retinal nerve fiber layer progression in glaucoma: A study on optical coherence tomography guided progression analysis," *Invest. Ophthalmol. Vis. Sci.* **51**(1), 217–222 (2010).
26. L. H. Lima *et al.*, "Structural assessment of hyper auto fluorescent ring in patients with retinitis pigmentosa," *Retina* **29**(7), 1025–1031 (2009).